Received: 2 August 2017 | Revised: 27 October 2017 | Accepted: 4 November 2017

DOI: 10.1002/cnm.2942

RESEARCH ARTICLE - FUNDAMENTAL

WILEY

Electro-mechanical response of a 3D nerve bundle model to mechanical loads leading to axonal injury

I. Cinelli[1,3] | M. Destrade[2] | M. Duffy[1] | P. McHugh[1]

[1]Discipline of Biomedical Engineering, NUI Galway, University Road, H91 TK33, Galway, Ireland

[2]School of Mathematics, Statistics and Applied Mathematics, NUI Galway, University Road, H91 TK33, Galway, Ireland

[3]Discipline of Electrical and Electronic Engineering, NUI Galway, H91 TK33, Galway, Ireland

Correspondence
Ilaria Cinelli, National University of Ireland Galway, Galway, Ireland.
Email: i.cinelli1@nuigalway.ie

Funding information
Galway University Foundation; Biomechanics Research Centre; Power Electronics Research Centre

Abstract

Traumatic brain injuries and damage are major causes of death and disability. We propose a 3D fully coupled electro-mechanical model of a nerve bundle to investigate the electrophysiological impairments due to trauma at the cellular level. The coupling is based on a thermal analogy of the neural electrical activity by using the finite element software Abaqus CAE 6.13-3. The model includes a real-time coupling, modulated threshold for spiking activation, and independent alteration of the electrical properties for each 3-layer fibre within a nerve bundle as a function of strain. Results of the coupled electro-mechanical model are validated with previously published experimental results of damaged axons. Here, the cases of compression and tension are simulated to induce (mild, moderate, and severe) damage at the nerve membrane of a nerve bundle, made of 4 fibres. Changes in strain, stress distribution, and neural activity are investigated for myelinated and unmyelinated nerve fibres, by considering the cases of an intact and of a traumatised nerve membrane. A fully coupled electro-mechanical modelling approach is established to provide insights into crucial aspects of neural activity at the cellular level due to traumatic brain injury. One of the key findings is the 3D distribution of residual stresses and strains at the membrane of each fibre due to mechanically induced electrophysiological impairments, and its impact on signal transmission.

KEYWORDS

coupled electro-mechanical modelling, diffuse axonal injury, equivalences, finite element modelling, trauma

1 | INTRODUCTION

Traumatic brain injury (TBI) is caused by mechanical loading to the head due to a sudden acceleration or a blast wave, for example, causing pathologies which range from focal damage of brain tissue to widespread axonal injury.[1,2] TBI in humans may result from falls, vehicle accidents, sport injuries, military incidents, etc.[1,3,4]

The diffuse form of TBI is called diffuse axonal injury (DAI), ie, a mechanical pathogenesis of an axonal injury, initiated in the deep white matter regions of the brain at the moment of injury.[1,3] DAI is the most common pathological feature of the mild and severe cases of TBI at cellular and subcellular levels,[1,5] with progressive course,[3] responsible for long-lasting neurological impairments following TBI, and high rates of mortality.[5-7] Pathological features of DAI include a wide-ranging variety of tissue lesions of the white matter (such as swelling of axonal mitochondria, thinning of the intermodal axoplasm, and development of myelin intrusions[8]), focal haemorrhages, contusions, and other brain injuries.[1,3,7]

Although DAI is classified as an independent category of disease from TBI, the pathological mechanism of DAI is very complex, and, currently, there are no diagnostic criteria.[3] A better understanding of mechanically induced electrophysiological impairments and damage associated with morphological changes of neural cells is urgently needed to improve diagnosis, clinical treatments, and prognosis.[3,7]

A number of experimental models of axonal injury reproduce DAI by experimental traumatic insult, where a traumatic axonal injury (TAI) induces DAI to investigate the relationship between mechanical forces and structural and functional responses of axons in experiments.[7] Experimental studies conducted on single axons[9] and nerve fibres[10] aim to induce TAI by applying pressure,[11,12] displacement,[1,10] strain,[9,13] shear strain,[14] and electroporation.[15] Although different types of loads seem to initiate TAI, recent studies have shown that the degree of neuronal impairment is directly related to the magnitude and rate of axonal stretch.[1,9,10,16] Beyond a critical threshold,[10] axons appear to be vulnerable to stretch-induced changes that induce morphological changes at the microscale level, increasing axolemma permeability.[1,3,5]

The alteration of axolemma permeability is evidence of mitochondrial damage and neurofilament compaction.[7,8] Axonal damage is a common manifestation of DAI. Injury-induced axonal damage involves damage of the axonal cytoskeleton, resulting in a loss of membrane integrity and impairment of axoplasmic transport, leading to changes in electrical signal propagation.[4,9,17] The alteration of neural activity in a mechanically injured nerve is called neurotrauma.[9,17,18] Although recent experimental studies highlight complex electro-mechanical phenomena at the nerve membrane layer,[19,20] the injury-induced electrophysiological changes of the electro-mechanical activity in neural cells are poorly understood.[7,9] Quantifying the induced electro-mechanical changes can help to differentiate severity of injury and to understand the alteration in signal propagation at cellular and nerve bundle levels.

Computational electro-mechanical models, coupling mechanics and electrophysiology, are powerful tools to investigate and evaluate neurophysiological, neuropathological processes, and neurocognitive damage associated with DAI due to injury at the macroscale.[1,2] This work presents a novel approach for evaluating and quantifying the changes in neural activity due to TAI by using finite element (FE) models. Previous modelling efforts have simulated 1-dimensional damage of a nerve fibre[2] and 2-dimensional axonal injury of brain tissue.[1] In this work, using the FE software Abaqus CAE 6.13-3, advanced 3-dimensional (3D) models explain the link between TBI and DAI at the microscale level,[1,2] by considering the case of TAI at the axonal and bundle levels. Our 3D FE model of a nerve bundle includes a representation of nervous cells made of extracellular media (ECM), membrane, and intracellular media (ICM). As in Cinelli et al,[21,22] these 3 regions have finite thicknesses, so that the resulting model is a 3-layer nerve bundle. Here, the bundle model is a section of an idealised geometry of a nerve bundle, which consists of 4 parallel cylindrical unmyelinated or myelinated fibres, see Figure 1. In this paper, a series of mechanical loads (such as pressure[11] and displacement[10]) are applied to the bundle to induce a certain level of damage at the nerve membrane of a fibre, altering the fibre activation dynamics and transmission.[16,17]

This model presents a unique framework for investigating how changes in strain and stress distributions alter the function of 3D myelinated and unmyelinated nerve fibres and bundles. In contrast to previous studies,[1,2] this model includes full coupling between mechanical and electrical domains[23,24] where the neural electrical activity, as described in Hodgkin and Huxley,[25] is coupled to the mechanical domain through piezoelectricity[20] and electrostriction,[19] reproducing biophysical phenomena accompanying the action potentials as observed experimentally.[20,26] Here, the electrical activity is directly coupled to mechanical deformation by using electro-thermal equivalences in a coupled thermo-mechanical FE analysis.[27] Electro-thermal equivalences and equivalent material properties have been shown to provide an efficient approach to resolve 3D electrical problems in a coupled electro-mechanical analysis in Abaqus CAE 6.13-3.[21,22]

This paper builds on the work reported in Cinelli et al.[21,23,24] Here, we report details of how electro-mechanical coupling is represented through thermo-mechanical equivalence; the nerve bundle model and its geometry; and the damage criterion and its implementation.

The electro-mechanical coupling approach is validated based on the strain-based damage criterion.[2,16,23] This criterion refers to traumatic mechanically induced damage on a nerve fibre (refer to Jérusalem et al[2] and Boucher et al[16]) in which the resting ionic potentials of the Hodgkin and Huxley (HH) model are shifted by 20 mV, simulating experimental evidence of damaged nerve fibres,[16,17] as in Jérusalem et al.[2] The injury threshold takes into account axonal strain along the nerve fibre length only.[1,2] The strain along the fibre length has been shown to be a physiologically relevant injury criterion for multiscale TBI models.[1,2] Two cases, (1) dynamic pressure and (2) displacement loads at the bundle level, in which only 1 fibre is activated, are considered.

This approach has the potential to generate useful insights in studying the mechanics behind neuro-physiology, as observed experimentally in damaged nerve membranes of clinical cases (such as multiple sclerosis).[9,18,28]

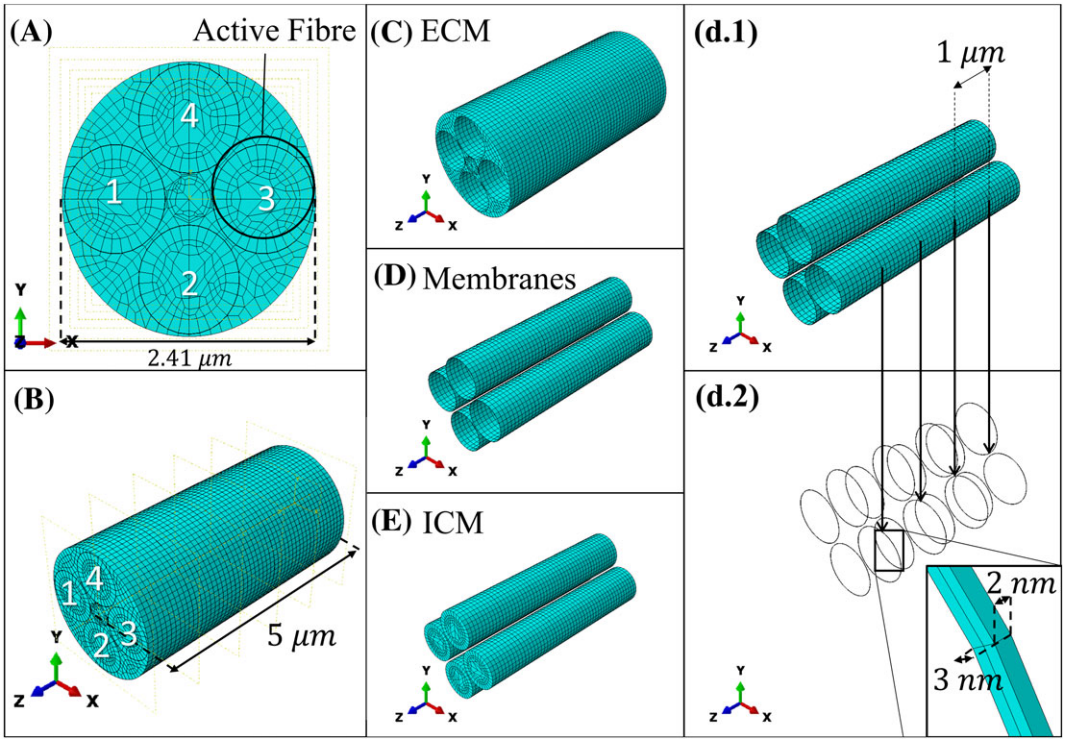

FIGURE 1 (A) Frontal view and (B) isometric view of the 3-layer nerve bundle, made of 4 fibres. Fibre #3 is the active fibre, ie, the fibre activated by a Gaussian voltage distribution.[26] Fibres #1, #2, and #4 are activated by the charges diffusing from Fibre #3. (C) The ECM, (D) the membrane, and (E) the ICM. In the case of myelinated fibres, the membrane layer is periodically partitioned along the fibre length to model the insulation sheath of the myelin layer, see (D.1), and the Ranvier's node, see (D.2). The myelin layer length is 1 μm, and the Ranvier's node length is 2 nm, while the radial thickness of the layer is equal to 3 nm[21,27,29]

2 | METHOD

2.1 | Electro-mechanical coupling

The electro-mechanical coupling of the action potential[25] is achieved through modelling of the nerve membrane as a piezoelectric material,[19] building on the equivalent electro-thermal modelling approach for predicting the electrical behaviour of nervous cells described in Cinelli et al.[21,23,27]

This can be described in terms of the piezo-elastic relation given in Equation 1 where $\boldsymbol{\varepsilon}$ is the total strain vector, $\boldsymbol{\beta}$ is the compliance matrix, $\boldsymbol{\sigma}$ is the mechanical stress vector, $\boldsymbol{\delta}$ is the piezoelectric strain coefficient vector, h is the thickness of the piezoelectric layer, and ΔV is the voltage difference across it.[30,31]

$$\boldsymbol{\varepsilon} = \boldsymbol{\beta}\boldsymbol{\sigma} + \boldsymbol{\delta}(\Delta V/h) \tag{1}$$

Similarly, the thermo-elastic strain-stress relation is described in Equation 2, where $\boldsymbol{\alpha}$ is the thermal expansion coefficients vector and ΔT is the temperature difference.[30,31]

$$\boldsymbol{\varepsilon} = \boldsymbol{\beta}\boldsymbol{\sigma} + \boldsymbol{\alpha}\Delta T \tag{2}$$

By the electro-thermal analogy,[23,27,30,31] the electric field, approximated here as the voltage across the membrane divided by its thickness, is equivalent to a thermal load, while the piezoelectric constants are equivalent to the thermal expansion coefficients, see Equations 1 and 2.

Simulating the nerve membrane as the dielectric component of a parallel plate capacitor,[25,30] the displacement follows the gradient of the electric field using the approach presented in Tawfik et al[30] and Staworko and Uhl,[31] see Equation 2. That is, the piezoelectric effect is only relevant in the through-thickness direction, represented here with orthotropic piezoelectric constants, approximately 1 nm per 100 mV[20] in the thickness direction and zero in the longitudinal and circumferential directions. Meanwhile, incompressible isotropic mechanical properties[26] are assumed.

As the electrical depolarization is initiated in the nervous cell,[25] compressive forces on the nerve membrane arise from piezoelectricity,[20] see Equation 2, leading to changes in shape (electrostriction[20,26,32]) and corresponding changes in capacitance. The electrical capacitance per unit area, C, changes as the square of the voltage,[21,26,32] see Equation 3 and Figure 2. Here, ϑ is the fractional increase in capacitance per square volt (equal to 0.036 V^{-2}[32]) and $\Delta\varphi$ is the surface potential difference (approximately −70 mV[32]).

$$C(V) = C(0)\left[1 + \vartheta(V + \Delta\varphi)^2\right] \tag{3}$$

Hence, this approach establishes a fully electro-mechanical coupling accounting, at the same time, for the effect of mechanical loads on electrical response and the effect of the electrical activity on the nerve structure.

2.2 | Model

The bundle model simulates the exchange of charges in 4 identical fibres as shown in Figure 1. Each fibre consists of a cylindrical region of ICM enclosed by a thin membrane and surrounded by a region of ECM.[27]

Two bundle models are used in this study: a fully unmyelinated bundle and a fully myelinated bundle. The neurite radii are $a_{ICM} = 0.477$ μm, $a_M = 0.480$ μm, and $a_{ECM} = 0.500$ μm[27] for the ICM, membrane, and ECM layers, respectively. As a first step, this analysis is focused on the radial distribution of charges rather than on longitudinal variations. The length of the bundle is 5 μm for a diameter equal to 2.41 μm in both cases, see Figure 1, within the range of the human optic axon.[33]

To model a myelinated fibre, we assume an ICM enclosed by a single layer, which is periodically partitioned along the fibre length, similarly to the histologic section of a myelinated fibre, see Figure 1 (D.1) and (D.2). The insulation sheath of myelin around the nerve fibre is modelled as an insulating layer, which replaces the membrane layer at regular

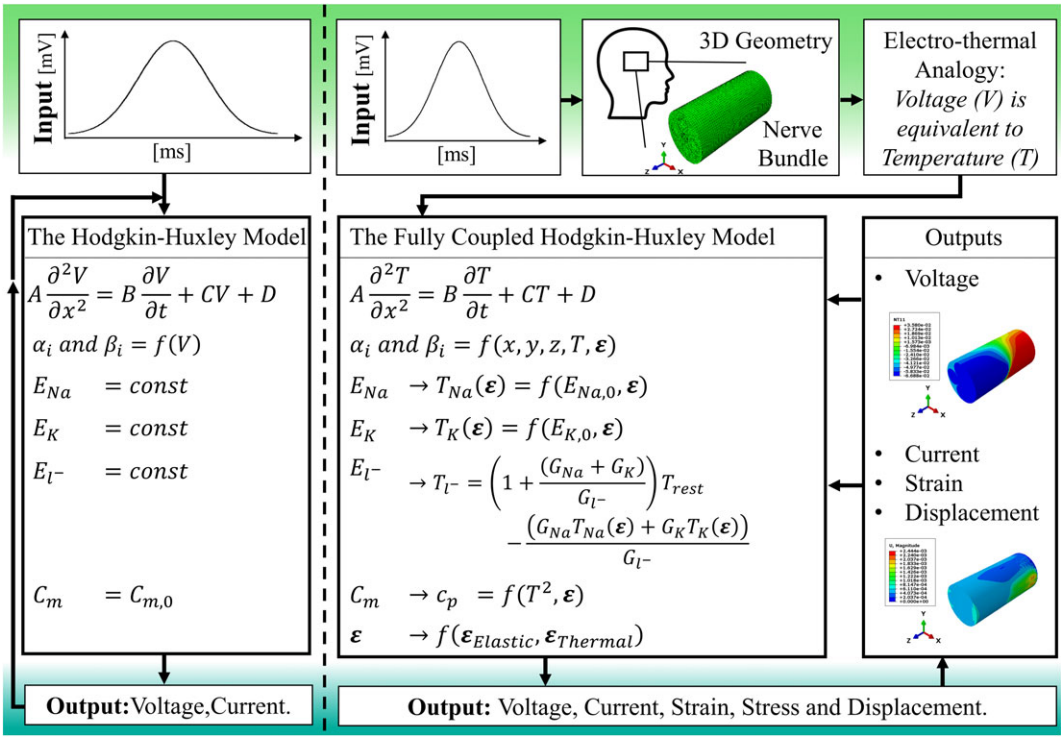

FIGURE 2 Flowchart of the code describing the active behaviour of the nerve's membrane: on the left, the HH dynamics[25] and on the right, the fully coupled HH dynamics. Here, a Gaussian voltage distribution elicits the action potential in a 3D model of a nervous cell. By using electro-thermal equivalences, the HH model is implemented as an equivalent thermal process, in which the membrane's conductivity changes as in Hodgkin and Huxley[25] and the capacitance, C_m, changes as in Alvarez and Latorre.[32] The HH parameters are changing based on the temperature (which is the equivalent quantity of voltage[21]) and strain at the membrane.[2] The strain ε generated in the model is a function of temperature, T, and thermal expansion coefficients, see Equations 3 and 4. Voltage, current, strain, and stress distribution are only a few of the 3D results released by Abaqus by equivalence

intervals along the fibre,[29] see Figure 1 (D.1). Different conductivity values are assigned to denote the myelin and membrane sections,[29] see Figure 1 (D.2). The width of the piecewise conductive membrane regions (or Ranvier's nodes) is 0.002 μm and the internode distance is 1 μm,[29] see Figure 1 (D.2).

Incompressible isotropic mechanical properties[26] are assumed in both models, with Young's Modulus equal to 1 GPa and a Poisson's ratio of 0.49[26] (close to incompressibility). Then, the electrical model parameters for unmyelinated and myelinated fibres are taken from, Jérusalem et al[2] and Cinelli et al[22], respectively. The resistance per unit length of the ICM and ECM is 1.89 Ωm, and for the myelin it is 4 MΩm. Then, the capacitance per unit area is 0.148 $\mu F/cm^2$ for the ICM, 3.54 $\mu F/cm^2$ for the ECM, and 3.58 10^{-3} $\mu F/cm^2$ for the myelin layer. The corresponding values for the membrane are the HH model values[25] for steady-state conditions and are dependent on voltage, strain, and spatial coordinates during loading conditions, see section D.

According to previous published work,[21,34,35] a neurite refers to a part of the body of a nervous cell (axon) that consists of two structurally distinct regions (axoplasm and membrane). By contrast, a *fibre* usually refers to an axon (axoplasm and membrane) with a myelin layer. In this work, neurite refers to a myelinated fibre too, because the myelin layer is modelled as periodical lengths of an insulating layer at the nerve membrane layer, whose radial extension has been neglected, as in Einziger et al.[29]

2.3 | Damage evaluation

Strain-based damage affects sodium and potassium reversal potentials ($E_{Na}(\varepsilon_m)$ and $E_K(\varepsilon_m)$), see Equation 4, of the HH model, simulating the changes in ionic concentration across the nerve membrane depending on the membrane strain (ε_m).[2] The resting potentials at physiological conditions are E_{Na0} and E_{K0}[2,25] see Equation 4. If a maximum strain, $\widetilde{\varepsilon}$, is exceeded, then the reversal potentials are zero; otherwise, the changes follow Equation 4 if $\varepsilon_m < \widetilde{\varepsilon}$[2]:

$$\begin{cases} E_{Na}(\varepsilon_m) = E_{Na0}(1-(\varepsilon_m/\widetilde{\varepsilon})^{\gamma}) \\ E_K(\varepsilon_m) = E_{K0}(1-(\varepsilon_m/\widetilde{\varepsilon})^{\gamma}) \end{cases}. \tag{4}$$

Here, the strain threshold, $\widetilde{\varepsilon}$, is set at 0.21 as an indicator of the onset of functional damage at which there is a 25% probability of having morphological injury during an uniaxial displacement test of a nerve fibre.[10] The parameter γ, equal to 2,[2] is an index referring to the sensitivity of the damage to small versus large deformation, see Jérusalem et al.[2] Additionally, the reversal potential of the leak ions E_{l^-} is not influenced by the strain but varies based on changes in gradient concentrations of potassium and sodium across the membrane,[2] see Figure 2. The changes for the leak ions can be derived from the sum of the total membrane currents at resting conditions.[2,25]

2.4 | Implementation

The implementation of the coupled HH model is shown in Figure 2 (on the right), in contrast to the uncoupled HH model (shown on the left). By using the electro-thermal equivalence,[23,27] the implementation of the neural activity, the distribution of voltage, and the generated strain can be seen in 3D by using well-established coupled thermo-mechanical software simulation tools. In the coupled model,[23] the membrane electrical conductivity changes in response to the membrane voltage produced during the action potential, incorporating the effects of strain,[2,25] according to Equation 4, while the electrical capacitance per unit area changes with the square of the voltage,[32] see Equation 3. The HH reversal voltage potentials change due to the strain at the membrane;[2,16] hence, the threshold of spike initiation changes as in Hodgkin and Huxley.[25] In all cases, strain is caused by membrane piezoelectricity as described in Equation 1, and external mechanical loading when applied. The model is implemented as a coupled thermo-mechanical model in Abaqus CAE by using user-defined subroutines (DISP, USDFLD, and UMATHT) to assign thermal equivalent electrical properties to the membrane of each fibre, independently, based on the spike initiation,[36] strain,[2,16] and voltage[32] generated at the same membrane, see Equations 2 and 3. Electrical model parameters for other regions of the unmyelinated and myelinated fibres are taken from, Jérusalem et al[2] and Cinelli et al,[22] respectively.

2.5 | Boundary conditions

In all cases, a voltage Gaussian distribution (with zero-mean and 0.4 variance) is the upper-threshold stimulation applied on Fibre #3 along its length, see Figure 2, while the other fibres are activated only if the diffused charges from Fibre #3

generate an input voltage higher than the modulated threshold.[36] The voltage is applied on the surface of the nerve membrane layer through the DISP user-subroutine in Abaqus CAE, as a thermal load (ie, equivalent to applied voltage[21]). The 3D distribution of charges on Fibre #3 modulates the activation of the other fibres, see Figure 1. First, the electro-mechanical coupling has been assessed and validated by activating Fibre #3 with a pre-imposed strain condition (corresponding to a coupled left-shift (LS) of 0 or 20 mV of the transmembrane voltage) assuming an intact or traumatised membrane, respectively, as in Jérusalem et al[2] and Boucher.[16]

An encastré boundary condition is enforced at the origin of each model, while no rotation or shear is allowed by fixing a point on the same side of the model. Then, two cases of mechanical loads applied at the bundle have been considered. As a first step to assess this novel coupling, only frequency-independent loading conditions are considered throughout, after the initial steady-state, so the solutions are quasi-static.[21] In the first case of applied mechanical loading, an instantaneous uniform compression is applied to the bundle to simulate injury conditions. Three values of pressure are modelled simulating mild (less than 55 kPa), moderate ($55-95$ kPa), and severe (higher than 95 kPa) pressure.[11] In the second case, axial strain conditions that reproduce the uniaxial test in[10] are applied. Two values of instantaneous uniform stretch are applied as a displacement boundary condition to simulate 5% and 14% of total axial deformation, ε, at which the probability of inducing morphological injury during the elongation test is 5% and 25%, respectively.[10]

2.6 | Validation

This work builds on the work reported in Cinelli et al,[21] in which the theory of the electro-thermal equivalences is validated (using both mathematical analysis and computational tools) and verified for the case of nervous cells.[21] Then, in Cinelli et al,[21] the uncoupled HH model[25] is validated and verified for voltage and current boundary conditions.

In this work, a further validation is needed to assess the coupled HH model in the 3D nerve bundle model. Our model includes Jérusalem et al,[2] as the most recent and completed reference available in literature. Thus, the coupling is verified against Jérusalem et al[2] and validated through output comparison with Jérusalem et al[2] and Boucher et al[16] and by replicating compression and elongation test as in experimental literature.[10,11]

Because previous works refer to 1D computational models,[2,16] the verification is carried out by comparison of output behaviours (of voltage and displacement) within the same model. Hence, the approaches in Jérusalem et al[2] and Boucher et al[16] are implemented in our 3D nerve bundle model for the same applied boundary conditions. Traumatic mechanically induced damage approach[2,16] is validated by using a coupled left-shift (*LS*) version of the HH model[16] reproducing experimental evidence,[16,17] as in Jérusalem et al.[2] The *LS* denomination refers to the induced positive shift of the transmembrane potentials, simulating a nerve membrane subjected to mechanical trauma.[2] It is called coupled *LS* to highlight the close link of mechanical strain on the electrical properties of the nerve membrane. In contrast to Hodgkin and Huxley,[25] the ionic currents of the modified HH model include the fraction of affected ionic channels by the strain (*AC*) and coupled *LS* variables, see Equations 5 and 6.[16] When a trauma occurs at the nerve membrane, the ionic resting potentials undergo a voltage-shift (*LS*), here, equal to 20 mV, as a reference value for trauma-induced kinetic changes observed in experiments.[16] This allows to simulate uniaxial loading experiments[13,37] of a nerve bundle, by implementing a pre-imposed shift in the HH dynamics, simulating the impact of applied mechanical strain at the nerve membrane. Then, the integrity of the nerve membrane is modelled as the fraction of the voltage-time dependent activation and inactivation variables (ie, m, n,and h[25]) of the HH model, shifted by *LS* (here, indicated as m_{LS}, n_{LS},and h_{LS}), see Equations 5 and 6.[16] The model accounts for the case where only a fraction of nodal channels (*AC*) undergoes a *LS*, while the rest of the membrane's channels, $(1-AC)$, remains intact.[16] Here, only the extreme cases of the entire membrane being traumatised ($AC=1$) or intact ($AC=0$) are shown as illustrative examples. In Equation 5, the sodium current, I_{Na}, and, in Equation 6, the potassium current, I_K.[16] The membrane potential is V_m, and the sodium, $\overline{g}_{Na}$, and potassium, $\overline{g}_K$,conductances are, respectively, equal to 120 and 36 $^{\mathrm{mS}}/_{\mathrm{cm}^2}$.[25]

$$I_{Na} = \left[m^3 h(1-AC) + m_{LS}^3 h_{LS} AC\right](V_m - E_{Na})\overline{g}_{Na} \tag{5}$$

$$I_K = \left[n^4(1-AC) + n_{LS}^3 AC\right](V_m - E_K)\overline{g}_K \tag{6}$$

This model is validated considering two cases of interest and two approaches. The first case (I) is the nerve membrane at physiological conditions, ie, intact ($LS=0$) and non-traumatised ($AC=0$). In second case (case II), the membrane loses integrity ($AC=1$) due to damage ($LS=20\ mV$). Then, in the first approach, the reversal ionic potentials in Equations 5

to 6, E_{Na} and E_K, are constant values, equal to 50 and −77 mV, respectively,[25] as in Boucher et al.[16] Here, the signals are changing because of the changes in conductance produced by changes in the voltage-dependent variables (m_{LS}, n_{LS},and h_{LS}). In a second approach, the reversal potentials are changing with *LS*, see Equation 4, as in Jérusalem et al.[2] Here, the signals are changing due to the changes in both the conductance and the reversal ionic potentials. Figure 3 shows the changes in membrane potential due to the left-shift voltage implemented as in Boucher et al[16] (indicated with *) and as in Jérusalem et al[2] (indicated as **). Those 2 conditions are the ones that can be directly compared with Jérusalem et al[2] and Boucher et al.[16]

All the equations of the electro-mechanical coupling are collected in the Appendix in greater details.

3 | RESULTS

3.1 | Model analysis

The electrophysiological impairments associated with structural damage of the neuron mechanics affect the electrostriction and the electric field across the membrane, Equation 3, while the piezoelectric properties of the nerve membrane are assumed to be constant, Equation 2.[20,21,26]

The results in Figure 3 confirm the ability of the model to reproduce the membrane voltage and ionic current waveforms of a damage-induced injury. Here, the coupled *LS* model of HH reproduces the changes in hyperpolarization in a damaged axon, left-shifting the affected ionic channels by 20 mV, as in slow-severe cases, as in Jérusalem et al[2] and Boucher et al.[16] Figure 3 refers to Fibre #3, the only fibre directly activated by the Gaussian voltage distribution input. Similarly, by diffusion, the membrane potential of the other fibres changes according to the level of damage and trauma on Fibre #3. Figure 3A shows the membrane potential, and Figure 3B reports the ionic currents of the membrane (for leak ions, I_{l^-}, potassium, I_K, and sodium, I_{Na}) vs time in Cases I, II (*), and II (**). As shown, the mechanically induced voltage shift of the resting potentials leads to a time-delay and a lower amplitude of the voltage signal, due to leaky channels, similar to trends observed in Jérusalem et al[2] and Boucher et al.[16] In Case II (*), the membrane potential is shifted by 13.3 ms, and its peak at 16.9 ms has a magnitude of approximately 10 mV. In Case II (**), the membrane potential is shifted by 13.7 ms, and the maximum magnitude is approximately −46.5 mV at 25.1 ms.

To illustrate the utility of the model in predicting the nerve mechanical response, Figure 4A,B shows the corresponding displacement vs time of an unmyelinated nerve membrane and myelinated nerve membrane, respectively, in a damaged bundle along the radial direction (ie, the $x-$ axis). Data are taken at the position of maximum radial displacement on Fibre #3. Figure 5 shows the total displacement distribution in an unmyelinated bundle (from (A) to (D)) and in a myelinated bundle (from (E) to (H)) with $LS = 20$ mV and $AC = 1$. In both cases, data are plotted at the time instant when the mechanical displacement is at its maximum.

For each case in Figure 3, residual compressive forces are found in unmyelinated and myelinated fibres, see Figures 4 and 5, due to the biophysical activity of the nerve membrane.[20,32] In an unmyelinated bundle, the displacement peak is −3.3 nm for Case I, −2.5 nm for Case II (*), and −0.6 nm for Cases II (**). In a myelinated bundle, the peak is −0.81 nm for Case II (*) and −0.27 nm for Case II (**). The peaks of the radial displacements occur at the membrane potential peaks for each case. In a myelinated bundle, lower displacements are found at the membrane than in the unmyelinated

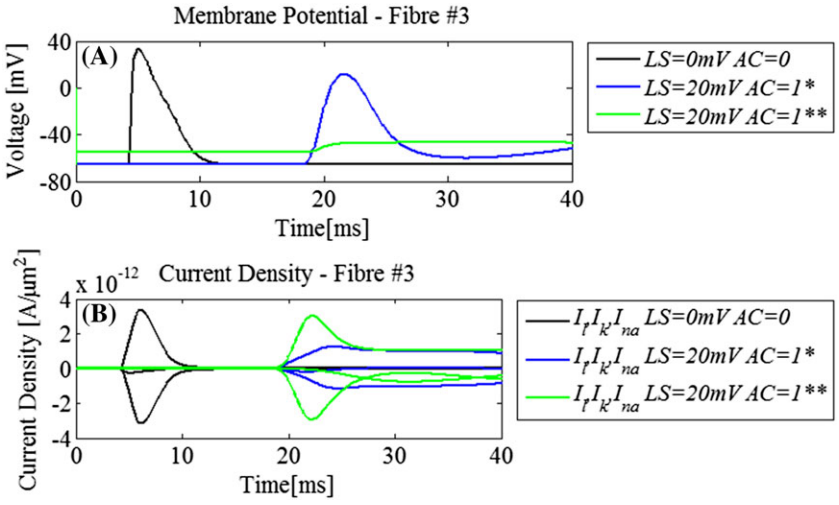

FIGURE 3 (A) The membrane's potential in case I, action potential ($LS = 0$ mV; $AC = 0$); case II, damaged traumatised membrane ($LS = 20$ mV; $AC = 1$). In *, the reversal ionic potentials have constant values as in Boucher et al,[16] and, in **, they change according to Equation 4, as in Jérusalem et al.[2] In (B), the current density [A/μm^2] on Fibre #3 for the cases considered

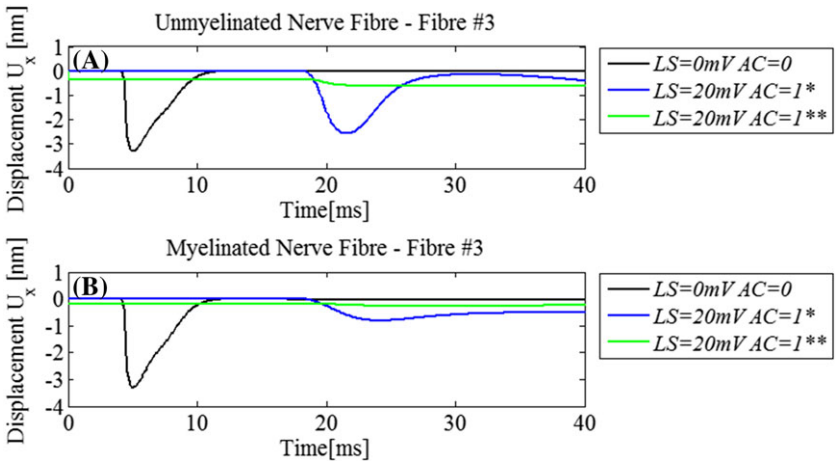

FIGURE 4 (A) Mechanical displacement of the unmyelinated nerve membrane; (B) displacement of a myelinated nerve membrane of the Fibre #3 in the 4 cases considered (see text) along the radial direction in the bundle (ie, the $x-axis$), U_x

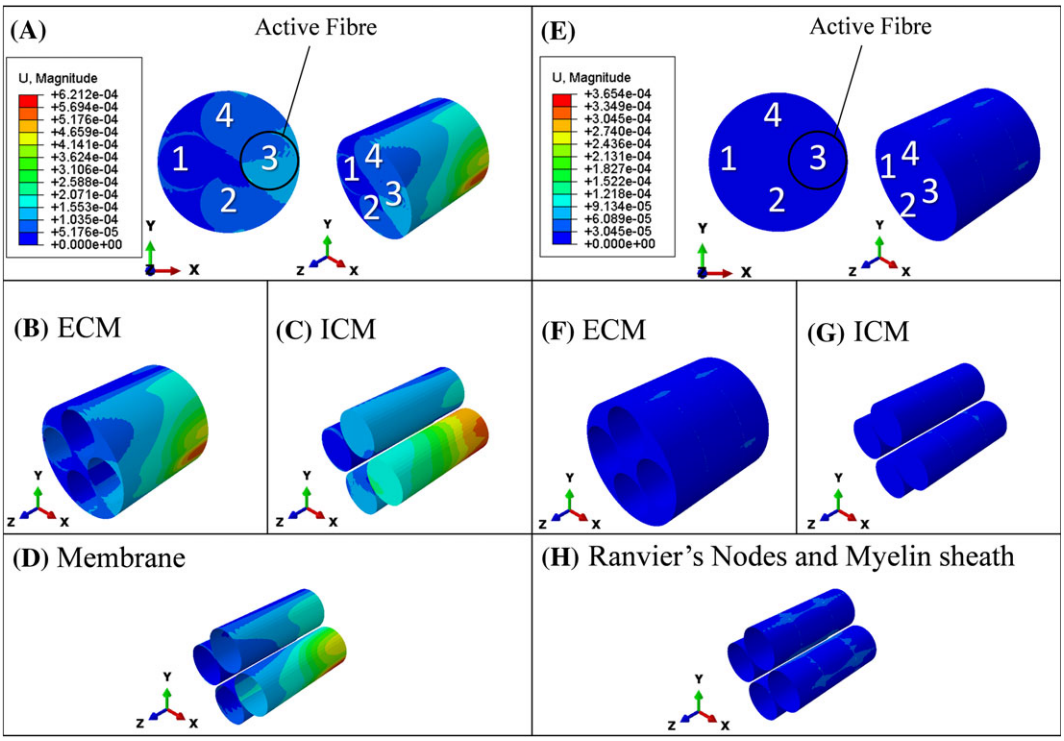

FIGURE 5 Frontal and isometric views of the total displacement in (A) an unmyelinated and (E) a myelinated nerve bundle model. In (B) and (F), the ECM; in (C) and (G), the ICM of the 2 bundle types. In (D), the isometric view of the nerve membrane and, in (H), the Ranvier nodes and the myelin sheath of the myelinated bundle. (A) to (D) and (E) to (H) are case II $(**)^2$ applied to an unmyelinated and myelinated nerve bundle. Data are taken at the peak of the membrane potential in both cases

case, see Figures 4B and 5E to H. The myelin layer constrains the deformation of the nerve membrane, reducing the displacement by approximately an order of magnitude on the same unmyelinated fibre, see Figures 4B and 5E to H. Assuming the Ranvier node regions are aligned in a bundle, the total displacement of the bundle is driven by the same deformation as the activated fibre, see Figure 5H.

3.2 | Mechanical loading cases of interest

In this section, the fully coupled electro-mechanical model of Figure 2 is applied to investigate different mechanical loading conditions directly using Equations 1 to 4, instead of as a simulated voltage shift.

3.2.1 | Pressure loads

Figure 6A,B shows the hyperpolarization and current densities of an unmyelinated bundle and a myelinated bundle under mild (25 kPa), moderate (68 kPa), and severe (192 kPa) pressures inducing TAIs.[11] The case of extreme pressure (1 GPa) is also considered. In contrast to the reference case of an intact nervous cell ($P = 0\ kPa$ and $AC = 0$), all pressure loads reduce the magnitude of the action potential and shift it over time, correlating with results in Figure 3. Here, the strain applied at the nerve membrane by compressing the bundle shifts the ionic resting potentials of the fully coupled HH model by a quantity which varies depending on the magnitude of the applied load, see Equation 4. Thus, only the AC variable is, here, considered.

Compression levels in the range of 25 to 192 kPa have a similar impact on the signal transmission both in terms of reduced magnitude and shift over time; this is found to be due to similar strain values read at the nerve membrane, because of the linear elastic assumption. In these cases, the peak of the membrane potential is approximately −17 mV with 16 ms of time-delay. Here, only slight differences are found for a traumatised vs non-traumatised nerve membrane ($AC = 1$ vs 0) when mild-to-severe pressures are applied, and therefore only results for $AC = 0$ are included, see Figure 6.

By contrast, application of extreme pressure changes the resting potential of ions reducing the current flow across the nerve membrane, see Figure 6B, and reducing the magnitude of the membrane potential to zero, see Figure 6A. An extreme pressure leads to both a reduction in magnitude and an increase of the voltage baseline up to −24 mV for an intact membrane, and up to −7 mV for a traumatised membrane, see Figure 6A,B. Here, the homeostatic balance of charges across the nerve membrane vanishes with an extreme pressure applied over a traumatised nerve membrane ($AC = 1$), because the strain levels at the nerve membrane are close to the threshold value assumed in Equation 4.

With mild-to-severe pressure loads from 25 to 192 kPa, the contraction of the nerve membrane due to the electrostriction has a similar trend to the case of $LS = 0$ mV and $AC = 1$, see Figure 3. Figure 7A,B shows the radial mechanical displacement on Fibre #3 of an unmyelinated and myelinated fibre, respectively. In both unmyelinated and myelinated bundles, the membrane potential is shifted through time durations by approximately 4.70 msec for the extreme pressure case (not shown here) and by 16.2 msec for the mild-to-severe cases,[11] respectively, see Figure 7 A,B. Higher deformation at the nerve membrane changes the ionic resting voltages leading to higher mechanical displacements, see Equation 4 and Figure 8.

Then, for the mild to severe cases of TAI-induced pressure,[11] the resting voltage potentials are changed due to the induced deformation in the bundle, and the magnitude of the action potential is, hence, reduced,[2] see Figure 7. The peak of the membrane potential is higher in a compressed unmyelinated bundle than in a compressed myelinated one.

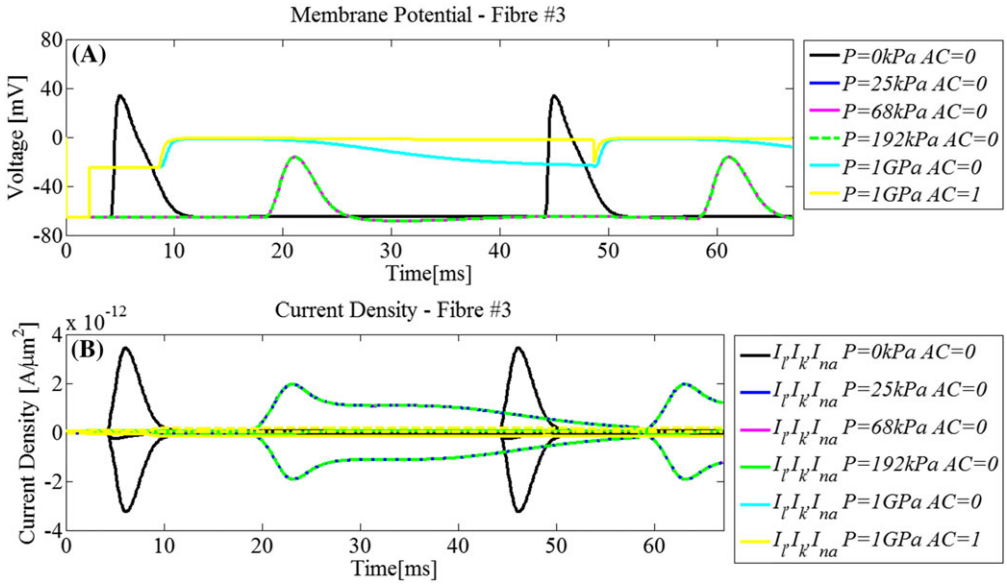

FIGURE 6 (A) Membrane potential $[mV]$ and (b) current density [A/μm^2] on Fibre #3 in the unmyelinated bundle under mild (25 kPa), moderate (68 kPa), and severe (192 kPa) pressures.[11] The extreme case of $P = 1$ GPa is also considered. AC is the fraction of affected ionic channels by the strain: $AC = 0$ is for an intact membrane and $AC = 1$ for a traumatised membrane.[16] Data are the maximum radial displacement of a node on Fibre #3

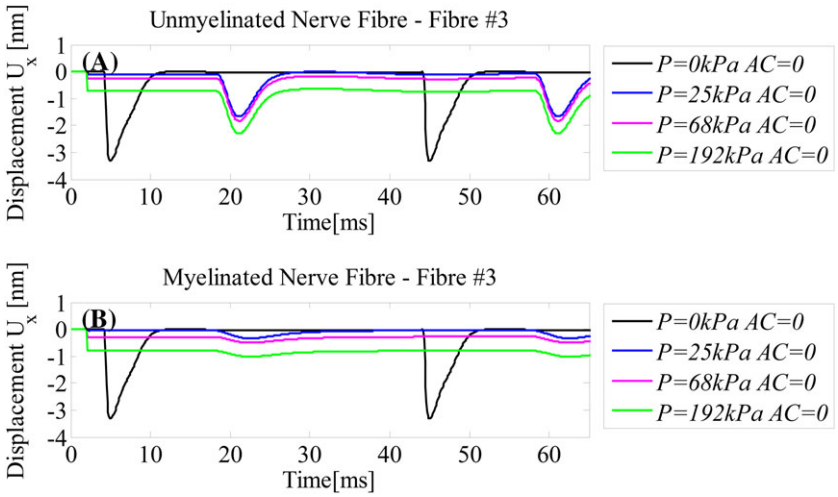

FIGURE 7 Radial displacement [nm] of (A) an unmyelinated bundle and (B) a myelinated bundle. Uniform applied pressures are classified as mild (25 kPa), moderate (68 kPa), and severe (192 kPa) pressures.[11] Data are the maximum radial displacement of a node on Fibre #3 in both cases

Within the range of pressure levels considered, an unmyelinated layer displaces according to the charges exchanged across the nerve membrane, see Figure 7. On Fibre #3, for the case of mild, moderate, and severe pressures, the peak is −1.67,−1.82, and −2.3 nm, respectively, while the peak of the reference case is at −3.4 nm, see Figure 7A. In a myelinated bundle, the charge-induced displacement of a myelinated fibre is much less than in an unmyelinated bundle, and therefore its displacement is more in response to the loading condition than to electrostriction, see Figure 7B. Here, on Fibre #3, for the cases of mild, moderate, and severe pressures, the peak is −0.34,−0.50, and −1 nm, respectively, see Figure 7B.

This model shows greater membrane displacements in an unmyelinated fibre than in a myelinated fibre, see Figure 7 A,B. The myelin layer constrains the deformation of the Ranvier nodes, which are the only regions throughout the fibre to show voltage-induced membrane displacement.[20] At the nodes, the applied compression acts in opposition to the electrostriction, because of the negative value of the membrane potential.

Then, the stresses are approximately $8.17 - 8.46$ MPa for $25 - 192$ kPa, with slight differences with AC. Shear are lower than the principal components.

3.2.2 | Displacement loads

In Figure 8A to B and 8C to D, a displacement boundary condition applied along the length of the unmyelinated and myelinated bundles, respectively, simulates 5% and 14% of total deformation.[7]

In an unmyelinated bundle, see Figure 8A to B and Figure 9A to D, the membrane potential is shifted through time durations by approximately 19 ms for $\varepsilon = 5\%$ and $AC = 0$, and by 21 ms for $\varepsilon = 5\%$ and $AC = 1$. For higher deformation, the membrane potential is delayed by 8 ms, showing similar results both with $AC = 0$ and $AC = 1$, representing the loss of ionic gradient across the nerve membrane, see Figure 8B. Then, the maximum of the membrane potential is approximately −64 mV for $\varepsilon = 5\%$ (with $AC = 0$ and $AC = 1$) and −60 mV for $\varepsilon = 14\%$ (with $AC = 0$ and $AC = 1$).

By contrast, in a myelinated bundle, see Figures 8B to D and Figure 9E to H, no significant differences have been found between intact and traumatised membranes. Here, for 5% and 14% deformation, the membrane potential is shifted up to −62 and −48 mV, respectively, while the peaks are shifted at 23 and 17 ms, respectively, see Figure 8C. Lower current density at the Ranvier nodes is mainly due to lower voltage gradient and higher localised strain, see Figures 8D and 9H.

Then, stresses are approximately 13 to 41.3 MPa, where the shear stresses are lower than the principal components.

4 | DISCUSSION

In contrast to previous studies,[1,2] this paper shows the advantages of a fully coupled electro-mechanical 3D framework to investigate the details of neural activity, combining real-time fully coupled electro-mechanical phenomena, modulated threshold for spiking activation, and independent alteration of the electrical properties for each fibre in the 3-layer nerve bundle, made of membrane (or Ranvier's nodes and myelin sheath), ICM, and ECM. The electro-mechanical coupling,

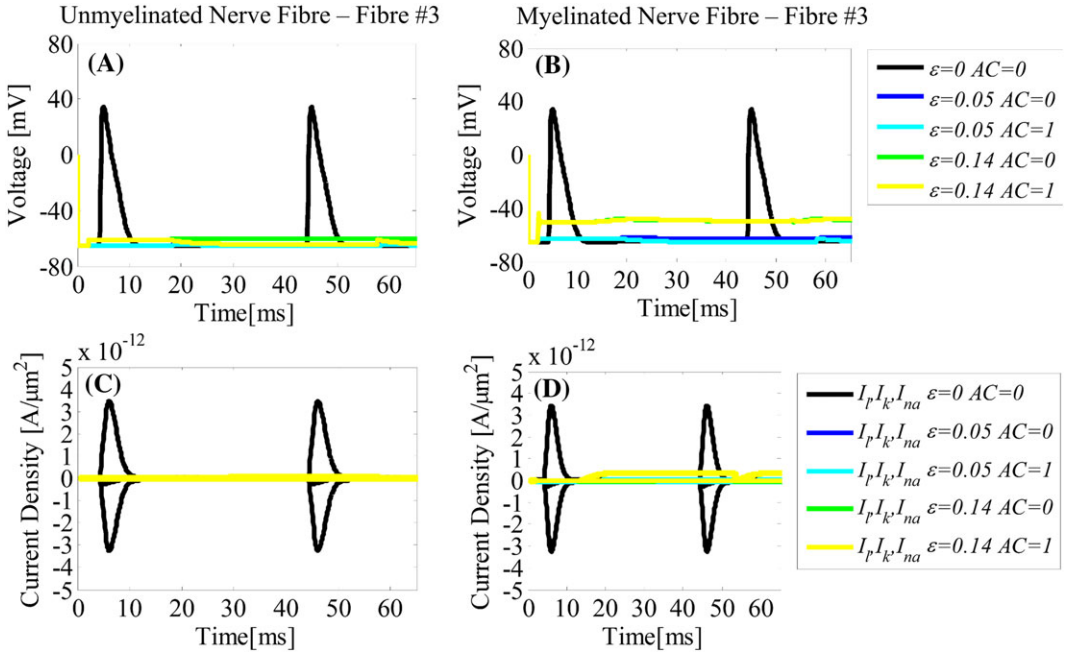

FIGURE 8 (A) to (B) Membrane potential [mV] and (C) to (D) current density [A/μm^2] on Fibre #3 in the unmyelinated bundle and myelinated bundle, respectively, under 5%and 14% of total deformation ε applied.[10] AC is the fraction of affected ionic channels by the strain: $AC = 0$ is for an intact membrane and $AC = 1$ for a traumatised membrane.[16] Data are taken at the maximum displacement along the bundle middle axis, ie, $z - axis$, on Fibre #3

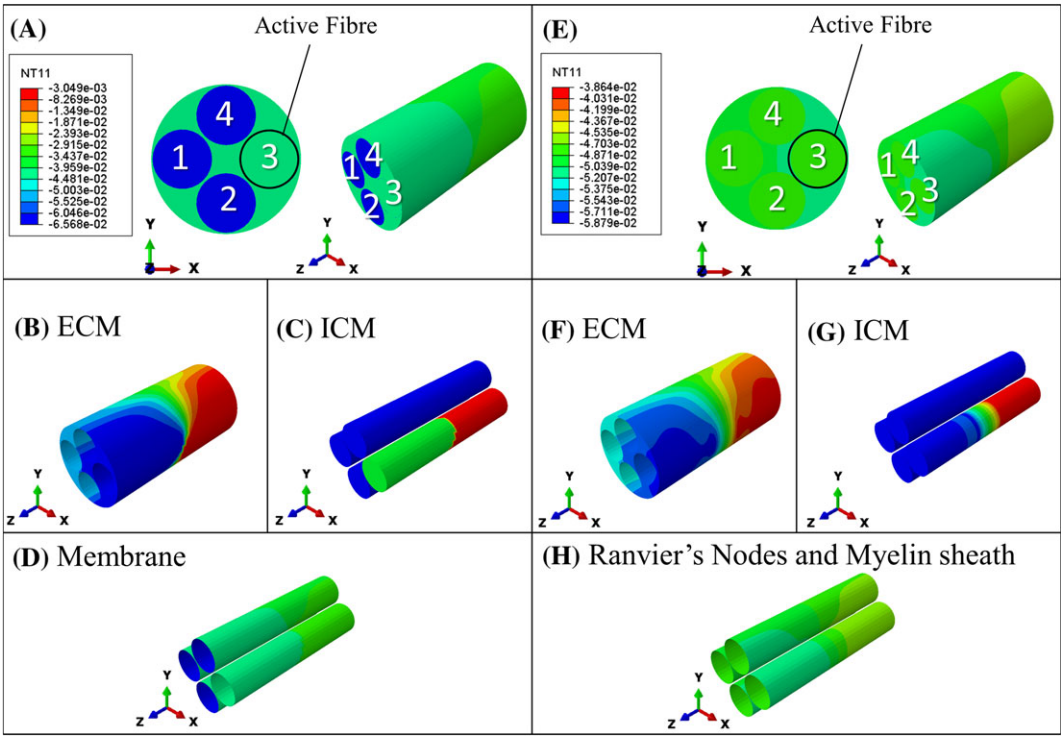

FIGURE 9 Voltage distribution (*NT*11) in an unmyelinated nerve bundle, in (A) to (D), and in a myelinated nerve bundle, in (E) to (H), for 5% elongation. Frontal and isometric view of an unmyelinated and myelinated nerve bundle model in (A) and (B), respectively. In (B) and (F), the ECM, in (C) and (G) the ICM of the 2 bundle types. In (D), the isometric view of the nerve membrane and, in (H), the Ranvier's nodes and the myelin sheath of the myelinated bundle

based on electro-thermal equivalences,[21,23,24,27] allows for reliable simulation of changes in electrostriction and neural activity due to mechanical damage, as seen in experiments.[10,11,16]

In this study, two cases of interest provide insights into the electrophysiological impairments of axonal injury due to sudden TAI-induced pressures and displacements. Differences in signal transition arise in the bundle for each fibre, depending on the fibre type. In the bundle, Fibre #3 is activated by imposing a voltage Gaussian distribution, while the other fibres are activated based on the voltage gradient from the active fibre and total strains (ie, elastic and thermal strain) read at the nerve membrane. Here, the nerve membrane integrity depends on the ionic resting potentials which are a function of the voltage and total strain at the nerve membrane. If the strains at the nerve membrane are lower than 0.21,[10] the resting voltage potentials change accordingly to the strain intensity. Alternately, no ionic gradient can be simulated at the membrane because the resting voltage values are zero,[2] as in the case of pressure higher than 192 kPa and elongation greater than 14%, see Figures 7 and 9.

During compression, unmyelinated nerve fibres show the greatest changes with mechanical loads due to the higher current density per area exchanged at the membrane, see Figure 7A. By contrast, lower density of ions per area can flow through the membrane at the Ranvier nodes, while the myelin layer constrains the electrostriction accompanying the neural activity, see Figure 7B. Then, during elongation, higher strains (along the bundle middle axis[2]) are read at the nerve membrane of unmyelinated fibres, while the myelin sheath protects the Ranvier's node regions by redistribution of the strains around the bundle, see Figure 8. In both cases, shear stresses are found to be lower than the principal components. However, future works might include shear as boundary conditions, due to the significance of the same in experimental literature.[38]

Results show that in the myelinated bundle the activation of the fibres is compromised because the fibre is not able to follow the pattern of activation under pressure and displacement loads. These two loading conditions are cases of clinical interest. A constant pressure on an axon is representative of injuries[1,3] and plaques in demyelinating diseases, acting as conduction block for action potentials of neighbouring axons inhibiting the myelinisation process. Instead, elongation tests might explain the relatively long time period needed for spontaneous membrane repair after fast strain.[13]

Finally, as highlighted earlier, the results refer to a cylindrical bundle made of 4 identical fibres with characteristics within the range of the human optic axon.[33] Although real nerve bundles are made of a higher number of fibres with different calibre,[33] the use of a simplified geometry was needed to assess electro-mechanical equivalences in a 3D FE model and to limit the computational cost. Ongoing work is focused on extending this technique to nerve bundles with different calibres (made of unmyelinated, myelinated, and mixed fibres) and activation of multiple fibres.

5 | CONCLUSION

We propose a fully coupled electro-mechanical framework for modelling the biophysical phenomena accompanying neural activity. Here, the coupling is based on an electro-thermal analogy by modelling the piezoelectric effect as a thermal expansion phenomenon in Abaqus CAE 6.13-3. This approach allows us to model and generate insights into aspects of neural activity, such as electrostriction and piezoelectricity, and to correlate these with experimental observations. The model, built on previously published work,[23,24,27] generates a fully 3D simulation of ion channel leaking for nerve fibres under pressure and displacement loads. In conclusion, in this model:

- Time-shift, signal magnitude, and nerve membrane potential baseline are dependent on the total strain, voltage, and size of the fibre;
- Lower strain and lower electrophysiological changes are found in myelinated fibre vs unmyelinated fibre;
- Unmyelinated fibre is needed to share information across the fibre, rather than throughout its length.

This model can contribute to understanding the causes and consequences of TBI and DAI to improve diagnosis, clinical treatments, and prognosis by simulating the mechanical changes accompanying the changes in signal transmission in TAI-induced loading conditions.

ACKNOWLEDGEMENT

The authors gratefully acknowledge funding from the Galway University Foundation, the Biomechanics Research Centre, and the Power Electronics Research Centre, College of Engineering and Informatics, National University of Ireland Galway (NUIG) in Galway, Rep. of Ireland.

ORCID

I. Cinelli http://orcid.org/0000-0003-1302-1188
M. Destrade http://orcid.org/0000-0002-6266-1221
M. Duffy http://orcid.org/0000-0002-1379-3279
P. McHugh http://orcid.org/0000-0001-9147-3652

REFERENCES

1. Wright RM, Ramesh KT. An axonal strain injury criterion for traumatic brain injury. *Biomech Model Mechanobiol*. 2012;11(1–2):245-260. https://doi.org/10.1007/s10237-011-0307-1
2. Jérusalem A, García-Grajales JA, Merchán-Pérez A, Peña JM. A computational model coupling mechanics and electrophysiology in spinal cord injury. *Biomech Model Mechanobiol*. 2014;13(4):883-896. https://doi.org/10.1007/s10237-013-0543-7
3. Ma J, Zhang K, Wang Z, Chen G. Progress of research on diffuse axonal injury after traumatic brain injury. *Neural Plast*. 2016;7. https://doi.org/10.1155/2016/9746313
4. Zhang YP, Cai J, Shields LBE, Liu N, Xu XM, Shields CB. Traumatic brain injury using mouse models. *Transl Stroke Res*. 2014;5(4):1-18. https://doi.org/10.1007/s12975-014-0327-0
5. Smith DH, Meaney DF. Axonal damage in traumatic brain injury. *Porg Clin Neurosci*. 2000;6(6):483-492.
6. Wang, H. C. and Ma, Y. Bin. Experimental models of traumatic axonal injury. *J Clin Neurosci*. 2010;17(2):157–162. https://doi.org/10.1016/j.jocn.2009.07.099
7. Delisi LE. Handbook of neurochemistry and molecular neurobiology. *Handb Neurochem Mol Neurobiol Schizophr*. 2010;27(1-2):107-241. https://doi.org/10.1016/j.jns.2009.03.019
8. Maxwell WL, Graham DI. Loss of axonal microtubules and neurofilaments after stretch-injury to guinea pig optic nerve fibers. *J Neurotrauma*. 1997;14(9):603-615.
9. Galbraith JA, Thibault LE, Matteson DR. Mechanical and electrical responses of the squid giant axon to simple elongation. *J Biomech Eng*. 1993;115(1):13-22. https://doi.org/10.1115/1.2895464
10. Bain AC, Meaney DF. Tissue-level thresholds for axonal damage in an experimental model of central nervous system white matter injury. *J Biomech Eng*. 2000;122(6):615-622. https://doi.org/10.1115/1.1324667
11. Hosmane S, Fournier A, Wright R et al. Valve-based microfluidic compression platform: Single axon injury and regrowth. *Lab Chip*. 2011;11(22):3888-3895. https://doi.org/10.1039/c1lc20549h
12. Gallant PE. The direct effects of graded axonal compression on axoplasm and fast axoplasmic transport. *J Neuropathol Exp Neurol*. 1992;51(2):220-230.
13. Shi R, Whitebone J. Conduction deficits and membrane disruption of spinal cord axons as a function of magnitude and rate of strain. *J Neurophysiol*. 2006;95(6):3384-3390. https://doi.org/10.1152/jn.00350.2005
14. LaPlaca MC, Cullen DK, McLoughlin JJ, Cargill RS. High rate shear strain of three-dimensional neural cell cultures: a new in vitro traumatic brain injury model. *J Biomech*. 2005;38(5):1093-1105. https://doi.org/10.1016/j.jbiomech.2004.05.032
15. Gallant PE, Galbraith JA. Axonal structure and function after axolemmal leakage in the squid giant axon. *J Neurotrauma*. 1997;14(11):811-822. https://doi.org/10.1089/neu.1997.14.811
16. Boucher PA, Joós B, Morris CE. Coupled left-shift of Nav channels: modeling the Na+-loading and dysfunctional excitability of damaged axons. *J Comput Neurosci*. 2012;33(2):301-319. https://doi.org/10.1007/s10827-012-0387-7
17. Yu N, Morris CE, Joós B, Longtin A. Spontaneous excitation patterns computed for axons with injury-like impairments of sodium channels and Na/K pumps. *PLoS Comput Biol*. 2012;8(9):e1002664. https://doi.org/10.1371/journal.pcbi.1002664
18. Geddes DM, Cargill RS, LaPlaca MC. Mechanical stretch to neurons results in a strain rate and magnitude-dependent increase in plasma membrane permeability. *J Neurotrauma*. 2003;20(10):1039-1049. https://doi.org/10.1089/089771503770195885
19. Mosgaard LD, Zecchi KA, Heimburg T. Mechano-capacitive properties of polarized membranes. *Soft Matter*. 2015;11(40):7899-7910. https://doi.org/10.1039/C5SM01519G
20. Zhang P-C, Keleshian AM, Sachs F. Voltage-induced membrane movement. *Nature*. 2001;413(6854):428-432. https://doi.org/10.1038/35096578
21. Cinelli I, Destrade M, Duffy M, Mchugh P. Electro-thermal equivalent 3D finite element model of a single neuron. *IEEE Trans Biomed Eng*. 2017;9294(99):1. https://doi.org/10.1109/TBME.2017.2752258
22. Cinelli I, Duffy M, McHugh PE. Thermo-electrical equivalents for simulating the electro-mechanical behavior of biological tissue. *Proc Conf IEEE Eng Med Biol Soc, EMBS*. 2015;3969-3972. https://doi.org/10.1109/EMBC.2015.7319263

23. Cinelli I., Destrade M, Duffy M, Mchugh P Neurotrauma evaluation in a 3D electro-mechanical model of a nerve bundle. In *Neural Engineering (NER), 2017 8th International IEEE/EMBS Conference on*, 2017: 2–5. https://doi.org/10.1109/NER.2017.8008402.
24. Cinelli I, Destrade M, Duffy M, Mchugh P. Electro-mechanical response of a 3D nerve bundle model to mechanical loads leading to axonal injury. In *Engineering in Medicine and Biology Society (EMBC), 2017 39th Annual International Conference of the IEEE*, 2017:1–4. https://doi.org/10.1109/EMBC.2017.8036989
25. Hodgkin AL, Huxley AF. A quantitative description of membrane current and its application to conduction and excitation in nerve. *J Physiol*. 1952;117(4):500-544.
26. El Hady A, Machta BB. Mechanical surface waves accompany action potential propagation. *Nat Commun*. 2015;6:6697. https://doi.org/10.1038/ncomms7697
27. Cinelli I, Duffy M, McHugh PE. Thermo-electrical equivalents for simulating the electro-mechanical behavior of biological tissue. In *37th Annual International Conference of the IEEE Engineering in Medicine and Biology Society (EMBC)*, 2015:3969–3972. https://doi.org/10.1109/EMBC.2015.7319263
28. Demerens C, Stankoff B, Logak M et al. Induction of myelination in the central nervous system by electrical activity. *Proc Natl Acad Sci U S A*. 1996:93(18):9887-9892. https://doi.org/10.1073/pnas.93.18.9887
29. Einziger PD, Livshitz LM, Dolgin A, Mizrahi J. Novel cable equation model for myelinated nerve fiber. *First Int IEEE EMBS Conf Neural Eng 2003 Conf Proceedings*. 2003;52(10):1632-1642. https://doi.org/10.1109/CNE.2003.1196769
30. Tawfik SA, Stefan Dancila D, Armanios E. Unsymmetric composite laminates morphing via piezoelectric actuators. *Compos Part A Appl Sci Manuf*. 2011;42(7):748-756. https://doi.org/10.1016/j.compositesa.2011.03.001
31. Staworko M, Uhl T. Modeling and simulation of piezoelectric elements—comparison of available methods and tools. *Mec Dent*. 2008;27(4):161-171.
32. Alvarez O, Latorre R. Voltage-dependent capacitance in lipid bilayers made from monolayers. *Biophys J*. 1978;21(1):1-17. https://doi.org/10.1016/S0006-3495(78)85505-2
33. Perge JA, Niven JE, Mugnaini E, Balasubramanian V, Sterling P. Why do axons differ in caliber? *J Neurosci*. 2012;32(2):626-638. https://doi.org/10.1523/JNEUROSCI.4254-11
34. Tahayori B, Meffin H, Dokos S, Burkitt AN, Grayden DB. Modeling extracellular electrical stimulation: II. Computational validation and numerical results. *J Neural Eng*. 2012;9(6):65006. https://doi.org/10.1088/1741-2560/9/6/065006
35. Meffin H, Tahayori B, Grayden DB, Burkitt AN. Modeling extracellular electrical stimulation: I. Derivation and interpretation of neurite equations. *J Neural Eng*. 2012;9(6):65005. https://doi.org/10.1088/1741-2560/9/6/065005
36. Platkiewicz J, Brette R. A threshold equation for action potential initiation. *PLoS Comput Biol*. 2010;6(7):25. https://doi.org/10.1371/journal.pcbi.1000850
37. Cao C, Yu A, Qin Q-H. Evaluation of effective thermal conductivity of fiber-reinforced composites. *Int J Arch Eng Const*. 2012;1(1):14-29. https://doi.org/10.7492/IJAEC.2012.002
38. Smith DH, Wolf JA, Lusardi TA, Lee VM, Meaney DF. High tolerance and delayed elastic response of cultured axons to dynamic stretch injury. *J Neurosci*. 1999;19(11):4263-4269.

How to cite this article: Cinelli I, Destrade M, Duffy M, McHugh P. Electro-mechanical response of a 3D nerve bundle model to mechanical loads leading to axonal injury. *Int J Numer Meth Biomed Engng*. 2018;34:e2942. https://doi.org/10.1002/cnm.2942

APPENDIX A.

The fully coupled Hodgkin and Huxley (HH) model reported in this work is based on the electro-thermal equivalences[21,22] and on the electro-mechanical coupling, see (A.3) and (A.4).

First, (A.1) and (A.2) show the implementation of the 3D Heat Diffusion Equation as the Cable Equation, see Cinelli et al.[21,22] The electrical material properties are substituted to the corresponding thermal properties, as discussed in Cinelli et al.[21,22] In the Heat Equation (A.1), T is the temperature [$^{\circ}C$ or K], ρ is the mass density [kg/m^3], c_p is the specific heat capacity [$J/(kg\ K)$], k is the thermal conductivity [$W/(mK)$], and Q is the heat source density [W/m^3]; correspondly, in the Cable Equation A.2 applied to the nerve, V_m is the transmembrane potential [V], S_v [$1/m$] denotes the surface-volume ratio, C_m [F/m^2] is the nerve membrane capacitance, σ [S/m] is the electrical conductivity of the membrane, and I_{ionic} [A/m] is the ionic current.

$$\rho c_p\, \partial T/\partial t - \nabla\cdot(\boldsymbol{k}\nabla T) + Q = 0 \tag{A.1}$$

$$C_m S_v \, \partial V_m/\partial t - \nabla\cdot(\sigma_e \nabla V_m) + S_v I_{ionic} = 0 \tag{A.2}$$

Secondly, (A.3) and (A.4) display the piezo-elastic strain-stress relationship vs the thermo-elastic strain-stress relationship, respectively (see Method—Section A).[2] In the electro-mechanical coupling, the piezoelectric strains are simulated by using the analogue thermo-mechanical quantity corresponding to the piezoelectric coefficients, ie, the thermal expansion coefficients $\boldsymbol{\alpha}$.[21]

$$\boldsymbol{\varepsilon} = \boldsymbol{\beta\sigma} + \boldsymbol{\delta}(\Delta V/h) \tag{A.3}$$

$$\boldsymbol{\varepsilon} = \boldsymbol{\beta\sigma} + \boldsymbol{\alpha}\Delta T \tag{A.4}$$

Then, simulating quasi-static solutions,[21] (A.5) shows the balance of ionic currents modelling the nerve membrane, as in the well-known HH model.[25]

$$\begin{aligned} C_M \frac{\partial V}{\partial t} &= \bar{g}_{Na} m^3 h (V - E_{Na}) + \bar{g}_K n^4 (V - E_K) + \bar{g}_l (V - E_{l^-}) = G_{Na}(V - E_{Na}) + G_K (V - E_K) + G_{l^-}(V - E_{l^-}) \\ &= I_{Na} + I_K + I_{l^-} \end{aligned} \tag{A.5}$$

Following trauma, electrical alterations can be due to the following: (1) the loss of integrity of the membrane[16] where a fraction of affected ionic channels (AC) is assumed to be traumatised; and (2) the transmembrane voltage shifts (LS) to positive values,[16] representing a different osmotic gradient due to the trauma-induced strains. The corresponding change in ionic currents for sodium, I_{Na}, potassium, I_K, and leak ions, I_{l^-}, are shown in (A.6), (A.7), and A.8, respectively (see Method—Section F). Then, the voltage-time dependent activation and inactivation variables of the HH model are m, n,and h.[25] The LS denomination refers to the activation and inactivation variables (here, indicated as m_{LS}, n_{LS},and h_{LS}) of the ionic gating channels affected by trauma.[16]

$$I_{Na} = \left[m^3 h(1 - AC) + m_{LS}^3 h_{LS} AC\right](V_m - E_{Na})\bar{g}_{Na} \tag{A.6}$$

$$I_K = \left[n^4(1 - AC) + n_{LS}^3 AC\right](V_m - E_K)\bar{g}_K \tag{A.7}$$

$$I_{l^-} = \bar{g}_{l^-}(V_m - E_{l^-}) \tag{A.8}$$

Additionally, the reversal potentials of potassium, A.9, sodium, A.10, and leak ions, (A.11), as the axonal component of the total strain applied at the bundle is changing (see Method—Section C).[2] The membrane resting potential is V_{rest}.

$$E_{Na}(\varepsilon_m) = E_{Na0}(1 - (\varepsilon_m/\tilde{\varepsilon})^\gamma) \tag{A.9}$$

$$E_K(\varepsilon_m) = E_{K0}(1 - (\varepsilon_m/\tilde{\varepsilon})^\gamma) \tag{A.10}$$

$$E_{l^-} = \left(1 + \frac{G_{Na} + G_K}{G_{l^-}}\right) V_{rest} - \frac{G_{Na} E_{Na}(\varepsilon_m) + G_K E_K(\varepsilon_m)}{G_{l^-}} \tag{A.11}$$

Finally, the electrical capacitance per unit area is changing with voltage as in (A.12) (see Method—Section A).[21,22]

$$C(V) = C(0)\left[1 + \vartheta(V + \Delta\varphi)^2\right] \tag{A.12}$$